

One-step Synthesis of Ultrasmall Platinum Nanoparticles Supported on Amino-Functionalized Graphene to Create an Electrochemical Molecularly Imprinted Polymer Sensor for Fluxapyroxad

Ling Shi¹, Jie Duan¹, Shufang Xu¹, Hongping Yang², Guangming Yang^{1,*}

¹ Engineering Research Center for Processing and Quality Control of Local Characteristic Food and Consumer Goods of High Education in Yunnan Province, College of Science, Honghe University, Mengzi 661199, PR China

² Library, Honghe University, Mengzi 661199, PR China

*E-mail: yangguangmingbs@126.com

Received: 22 February 2021 / Accepted: 15 April 2021 / Published: 31 May 2021

In this work, a novel electrochemical molecularly imprinted polymer (MIP) sensor for fluxapyroxad (FP) was constructed. This MIP sensor was based on indole-6-carboxylic acid (6-IAA) and platinum (Pt) nanoparticles (NPs) supported amino-functionalized graphene (NH₂-r-GO). Massive and ultrasmall Pt NPs (2-3 nm) were supported on NH₂-r-GO, which was easily prepared using a simple, aqueous phase method. Pt NP was firstly generated using ascorbic acid as the reductant and hexadecylpyridinium chloride as the structure-directing agent; then, NPs were immediately loaded on the surface of the coexisting NH₂-r-GO. Loading allowed for the interreaction between the amino group and Pt to form the hybrid nanocomposite. This hybrid material was then used to modify a glassy carbon electrode (GCE) surface, resulting in a Pt-NPs-NH₂-r-GO / GCE. After this modification, FP was imprinted on the aforementioned electrode surface using cyclic voltammetry, with 6-IAA as the functional monomer. Finally, FP was eluted from the polymer, resulting in the MIP sensor. After rebinding the template molecules Fe(CN)₆^{3-/4-} was used to measure the impedance of the MIP sensor. Results indicated an excellent response for FP across a linear range of 1.0×10⁻⁹ to 1.3×10⁻⁵ mol L⁻¹; the detection limit was determined to be 1.0×10⁻¹⁰ mol L⁻¹ (S/N= 3). This sensor was also used to detect FP in real samples, with results indicating it was a reliable sensor for FP.

Keywords: Electrochemical sensor; Fluxapyroxad; Molecularly imprinted polymer; Indole-6-carboxylic acid; Pt nanoparticles; Amino group functionalized-graphene

1. INTRODUCTION

Fluxapyroxad (FP) belongs to pyrazole fungicides, which is a new group of pesticides that are widely used to control fungal diseases in agricultural products [1]. Notably, FP has an inherently high

chemical stability, resulting in extensive residues after its use both on food and in the environment. Critically, these residues cause a variety of unpredictable risks to human health [2, 3]. Based on these potential health effects, many countries have set a maximum residue limit for FP in their food-safety control programs [3, 4]. Given this, it has become necessary to construct a sensitive and effective analytical method for monitoring FP residues in food products.

Currently, gas chromatography-tandem mass spectrometry (GC-MS / MS) [4] and liquid chromatography-tandem mass spectrometry (LC-MS / MS) [5, 6] have all been used to determine FP residues in food samples. These techniques have been used owing to their high precision and sensitivity; however, these methods usually involve tedious protocols and high costs. Thus, an electrochemical method would offer an alternative approach, owing to its advantageous simplicity, low cost, and high sensitivity when compared with traditional methods (e.g., GC-MS / MS and LC-MS / MS) [7-9]. Despite this potential, there remains no published work on the application of electrochemical methods to determine FP residues.

Electrochemical molecularly imprinted polymer (MIP) sensors have become a popular tool for the detection of pesticides. The performance of MIP sensors, including their respective sensitivities and selectivities, are closely related to the exposure of the imprinted sites on the sensing interface [7, 10]. Given this, using a surface imprinting is a promising strategy to improve the total amount of imprinted sites [11, 12]. Electrochemical polymerization has been widely used to prepare MIPs on an electrode surface. This approach has also been viewed as an ideal surface imprinting method, since it is simple, controllable, and highly efficient [12]. Moreover, conductive nanomaterials that have large, specific surface areas, such as graphene (r-GO), carbon nanotubes, metal nanomaterials, and their hybrid composites, would provide a large surface area for imprinting polymerization and allow for fast mass transfer [10, 11]. At the same time, the structure of the polymer is also an important factor for their performance. Regarding these polymers, polyaniline, polypyrrole, polythiophene, and their derivatives typically have tight structures, which reduce mass transfer and specific recognition sites [12]. Recently, we reported a MIP sensor for florfenicol based on poly-indole-5-carboxylic acid, which presented with a three-dimensional, porous structure [13]. Given these preliminary findings, further work is needed regarding the utility of a porous polymer for MIP-based sensors.

The hybrid nanocomposites of graphene (r-GO) and metal nanoparticles (NPs) have attracted a strong scientific interest for their use in electrochemical MIP sensors. This interest has been driven largely by their intrinsic physical properties, such as their high electrical conductivities, large surface areas, and excellent electrochemical performance as well as their chemical characteristics (e.g., modifiable surface and functional groups) [14-16]. Given this and to improve its properties, r-GO has been typically used as a supporter to load NPs. There are two main strategies to form these composites: (1) Mixing as-prepared materials and (2) using an *in situ* preparation method. In generally, the latter offers more advantages, including a fast, efficient, and easy process. However, the supported amount of NPs on the r-GO surface have typically been insufficient, with correspondingly large diameters [14, 16, 17]. As a result, this approach has remained challenging.

In this work, Pt NPs with a small diameter (2-3 nm) were prepared using hexadecylpyridinium chloride (HDPC) as the structure-directing agent. These Pt NPs were then loaded *in situ* on the surface of NH₂-r-GO to form a hybrid, nanocomposite of Pt-NPs-NH₂-r-GO that featured an interreaction

between the amino group and Pt. After, the hybrid material was used to modified electrode. FP was imprinted on above modified surface using cyclic voltammetry (CV), with indole-6-carboxylic acid (6-IAA) as the functional monomer and FP as the template molecule. Using this approach, a MIP electrochemical sensor for FP was successfully achieved. For this strategy, the massive, ultrasmall Pt NPs were easily supported on the NH₂-r-GO surface using a one-step synthesis. To our knowledge, this is the first time 6-IAA has been used as a monomer for MIP; it is also the first time an electrochemical MIP sensor for FP has been constructed.

2. MATERIALS AND METHODS

2.1 Chemicals

NH₂-graphene (NH₂-r-GO) was obtained from Nanjing XFNANO Materials Tech Co., Ltd. (Nanjing, China). Hexadecylpyridinium chloride monohydrate (C₅H₅N(Cl)(CH₂)₁₅CH₃·H₂O, HDPC, 99.0%), Chloroplatinic acid (H₂PtCl₆), indole-6-carboxylic acid (6-IAA, 99.0%), fluxapyroxad (99.9%), ascorbic acid (C₆H₈O₆, AA, 99.0%), bixafen (99.9%), and pyraclostrobin (99.9%) were all obtained from J&K Scientific Ltd. (Beijing, China). The phosphate buffer solution (PBS, pH=5.8) was prepared with Na₂HPO₄ and NaH₂PO₄, and this buffer was used to dissolve FP to prepare a FP stock solution. Purified water (18 MΩ cm⁻¹) was used in all experiments.

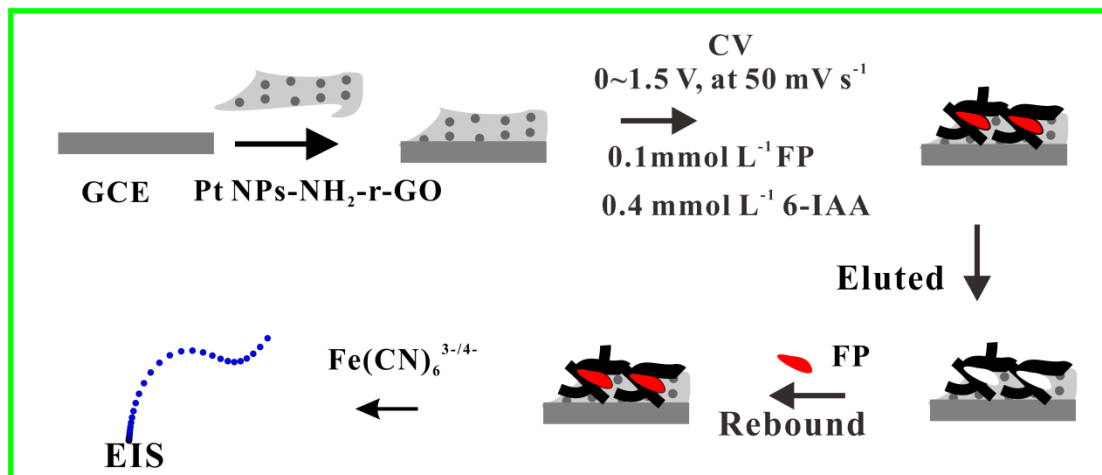
2.3 Synthesis of Pt-NPs-NH₂-r-GO

Briefly, 40 mg HDPC was dispersed in 10 mL NH₂-r-GO suspension (1.0 mg mL⁻¹). Then, 0.8 mL of 10 mmol L⁻¹ H₂PtCl₆ was added into above solution to obtain a homogeneous dispersion. In succession, 0.60 mL of AA (0.10 mol L⁻¹) was added into above dispersion, and kept undisturbed at 90°C for 3 h. The products were harvested via centrifugation and washed three times with H₂O and ethanol, respectively. Finally, the product was redispersed with H₂O, yielding a 1 mg mL⁻¹ Pt-NPs-NH₂-r-GO suspension.

2.4 Preparation of the MIP electrochemical sensor

The preparation of the MIP sensor is shown in Scheme 1. First, 5 μL 1 mg mL⁻¹ of Pt-NPs-NH₂-r-GO suspension was dropped onto the clean GCE surface, after which it was dried under an infrared lamp to obtain Pt-NPs-NH₂-r-GO / GCE. Then, Pt-NPs-NH₂-r-GO / GCE was immersed in an acetonitrile solution containing template molecule (FP, 0.1 mmol L⁻¹), functional monomer (6-IAA, 0.4 mmol L⁻¹), and electrolyte (tetrabutylammonium perchlorate, 0.1 mol L⁻¹). Afterwards, CV measurements were performed with Pt NPs-NH₂-r-GO / GCE as working electrode using a scan rate of 50 mV s⁻¹ and a potential range of 0 to 1.5 V. After 16 cycles, the resulting electrode was immersed in a methanol / acetic acid (9 / 1, V / V) solution for 20 min to elute the template molecule. After immersion, the final MIP / Pt NPs-NH₂-r-GO / GCE was produced. The non-imprinted polymer (NIP)

sensor was prepared using the same preparation conditions as the MIP sensor, with exception that no template was used. MIP-NH₂-r-GO / GCE was also fabricated identical to MIP / Pt NPs-NH₂-r-GO / GCE, but its polymerized substrate was NH₂-r-GO / GCE.



Scheme 1. The Scheme for the construction of MIP sensor.

2.5. Electrochemical measurements

MIP / Pt NPs-NH₂-r-GO / GCE was immersed in a 10 mL FP aqueous solution (pH=5.8) under mild magnetic stirring to allow recognition of the template molecules. After 400 s, the MIP / Pt NPs-NH₂-r-GO / GCE was rinsed with H₂O and immersed in a Fe(CN)₆^{3-/4-} aqueous solution containing 2.5 mmol L⁻¹ K₃Fe(CN)₆, 2.5 mmol L⁻¹ K₄Fe(CN)₆, and 0.1 mol L⁻¹ KCl. This was then used as the working electrode in subsequent electrochemical impedance spectroscopy (EIS) measurements.

3. RESULTS AND DISCUSSION

3.1 Morphology and structure of Pt NPs-NH₂-r-GO

Firstly, transmission electron microscopy (TEM) was used to record the morphological structure of the as-prepared products. TEM images of NH₂-r-GO indicated a characteristic wrinkled structure and either single or thinly layered sheets (Figure 1A). Results indicated that a large amount of Pt NPs were loaded on its surface (Figure 1B); the diameters of Pt NPs were 2-3 nm (Figure 1C). As previously described, Pt NPs were first synthesized under the structure-directing effect of HDPC; then, the NPs were immediately loaded onto the NH₂-r-GO surface. This loading occurred because of the interreaction between the amino group and Pt. This is different from our previous report, which showed the formation of a three-dimensional, porous Pt frame structure [18]. In this previous work, the structure formed in the absence of NH₂-r-GO in the reaction solution and was attributed to an

interreaction that was stronger than the directing effect of HDPC in the formation of the frame structure.

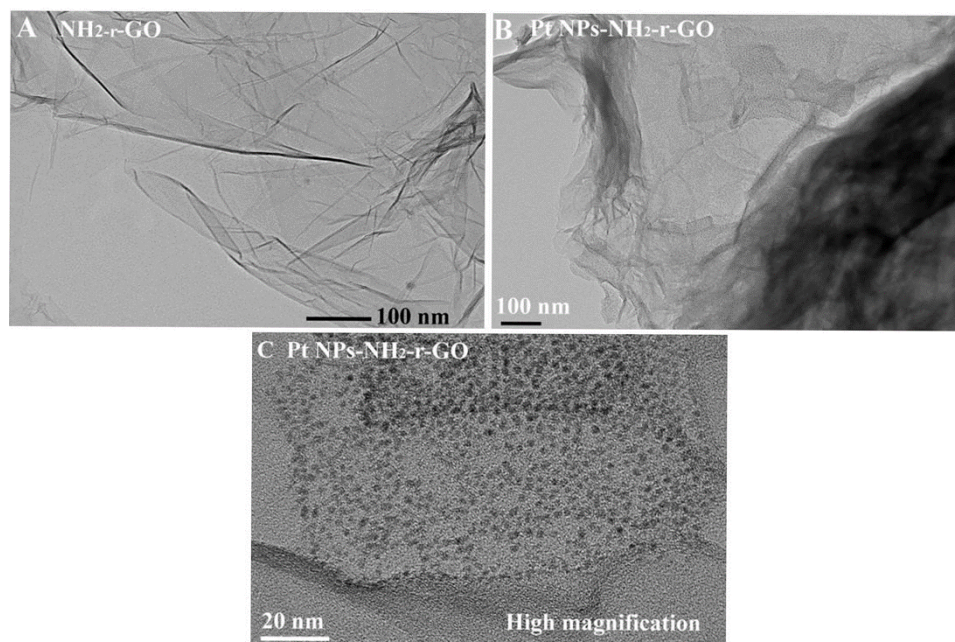


Figure 1. TEM images of NH₂-r-GO (A) and Pt NPs-NH₂-r-GO (B-C).

Next, scanning electron microscope (SEM) images of Pt NPs-NH₂-r-GO / GCE also indicated a characteristic wrinkled structure, which was in accordance with its TEM images. When MIP was successfully prepared on Pt NPs-NH₂-r-GO / GC (Figure 2A), its SEM image indicated porous, three-dimensional networks (Figure 2B). These network diameters were approximately 100 nm and were visually apparent even at low magnification image (Figure S1). Importantly, this finding was notably different from our previous report, which used 5-IAA as a functional monomer (Figure S2) [13]. This difference is attributed to the changing of the group position of the monomer. It is hypothesized that this structure provides benefits, including improved imprinted sites, accelerated mass transfer, and enhanced specific surface areas in comparison to the MIP based on polypyrrole, polythiophene, and their derivatives, which usually present a rapidly forming and intense structure. This MIP had a better group in the form of -COOH relative to the structures of polypyrrole, polythiophene and their derivatives. The inclusion of this group likely enhanced the interactions with other groups in the FP molecular structure (e.g., -NH, -C=O, and -C-N). Ultimately, this endowed as-prepared sensor with higher sensitivity and selectivity.

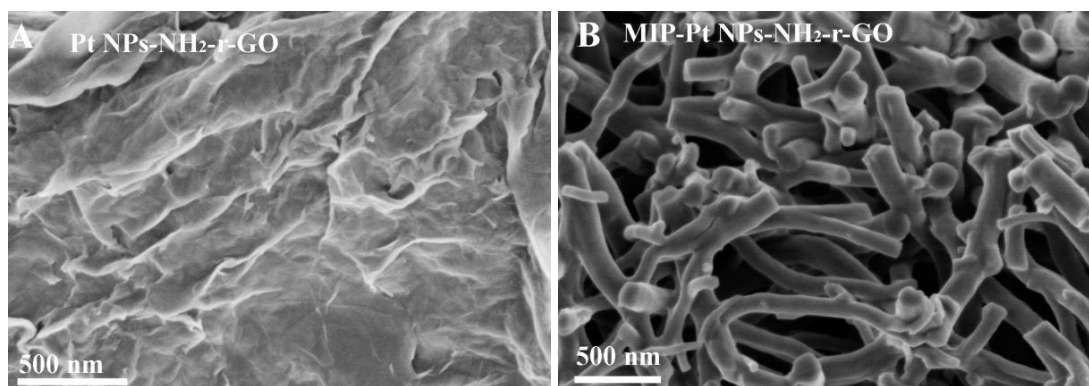


Figure 2. SEM images of Pt-NH₂-r-GO / GCE (A) and MIP-Pt NPs-NH₂-r-GO / GCE (B).

3.2 EISs of the modified electrodes

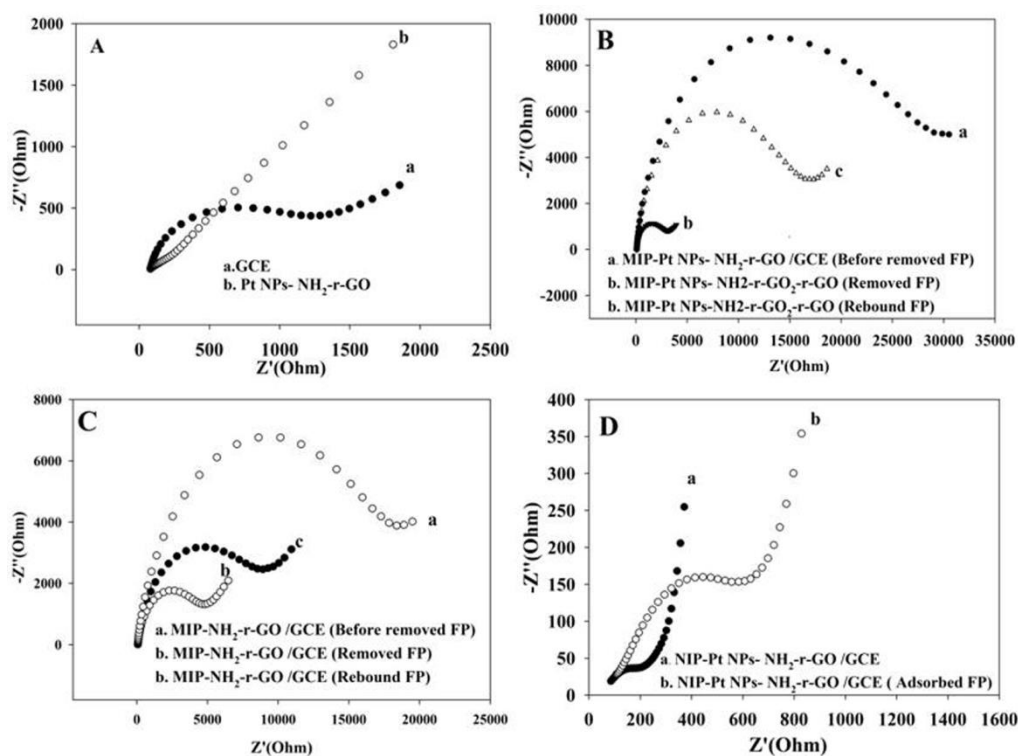


Figure 3. (A) EISs of GCE (a) and Pt-NPs-NH₂-r-GO / GCE (b). (B) EISs of MIP / Pt NPs-NH₂-r-GO / GCE as polymerized (a), eluted (b) and after rebound in 1.0×10^{-6} mol L⁻¹ FP (c). (C) EISs of MIP -NH₂-r-GO / GCE as polymerized (a), eluted (b) and after rebound in 1.0×10^{-6} mol L⁻¹ FP (c). (D) EISs of MIP / Pt NPs-NH₂-r-GO / GCE as polymerized (a) and after adsorbed in 1.0×10^{-6} mol L⁻¹ FP (b). Note: Test solution of EIS was 10 mL of 1.0 mmol L^{-1} K₃Fe(CN)₆+K₄Fe(CN)₆ containing 0.1 mol L^{-1} KCl.

The construction of the MIP sensor was determined and its performance was evaluated using EIS measurements. As shown in Figure 3A(a), the bare GCE presented a low value of electron-transfer resistance (Ret) (approximately 1200 Ω), however, the EIS of Pt NPs-NH₂-r-GO / GCE was almost a

straight line (Figure 3A(b)), indicating it enhanced the conductivity of the electrode. When MIP was polymerized on the above interface, the resulting electrode had a high Ret value (Figure 3B(a)); however, when the templates were eluted from MIP, the Ret decreased (Figure 3B(b)). This result indicated the recognition sites were formed in the polymer itself [19]. When MIP-Pt NPs-NH₂-r-GO / GCE was used to rebind FP (1×10^{-6} mol L⁻¹), its Ret value notably increased (Figure 3B(c)), indicating that the MIP had been successfully produced. For MIP-NN₂-r-GO /GCE (Figure 3C(a-c)), this change became smaller relative to that of MIP-Pt NPs-NH₂-r-GO / GCE. The reason for this change was due to the effect of Pt NPs, which enhanced the polymerization area and electron transfer capability. This then increased the recognition sites and signal amplification [20, 21]. As shown in Figure 3D (a-b) and regarding the NIP / Pt NPs- NH₂-r-GO / GCE, the change in Ret was approximately 400 Ω, indicating there were few, non-specific recognition sites that appeared on this interface.

3.3 Analytical performance of MIP sensor

To obtain the optimal response of the MIP sensor for FP, a series of experimental variables were next investigated, including mole ratio of FP to 6-IAA, electrochemical polymerization time, and adsorption time. Further detail regarding these variables is shown in SI (Figure S3). As shown in Figure 4A, the MIP-Pt NPs-NH₂-r-GO / GCE Ret increased with increasing FP concentration; moreover, in the range of 1.0×10^{-9} to 1.0×10^{-6} mol L⁻¹ and 1.0×10^{-6} to 1.3×10^{-5} mol L⁻¹, it exhibited an evident linear response. The regression equations were $Z'(\Omega) = 3670 + 8587 C$ ($\mu\text{mol L}^{-1}$), $r^2 = 0.9930$) and $Z'(\Omega) = 10082 + 1217 C$ ($\mu\text{mol L}^{-1}$), $r^2 = 0.9951$) (Figure 4 B), respectively. The detection limit was 1.0×10^{-10} mol L⁻¹ (S/N= 3). Importantly, this sensor possessed a lower detection limit for compared to GC-MS / MS [4] and LC-MS / MS [5, 6, 22], the details were shown in Table 1.

Table 1. Comparison between the proposed MIP sensor with those reported in the literatures for FP detection

methods	Linear range ($\mu\text{mol L}^{-1}$)	Limit of detection ($\mu\text{mol L}^{-1}$)	Ref.
GC-MS/MS	0.001 ~ 0.025	0.0005	[4]
LC-MS/MS	0.0125 ~ 25	0.005	[5]
LC-MS/MS	0.0025 ~ 0.25	0.0025	[6]
LC-MS/MS	0.00025 ~ 0.025	0.00125	[22]
MIP sensor	0.001~ 13	0.0001	This work

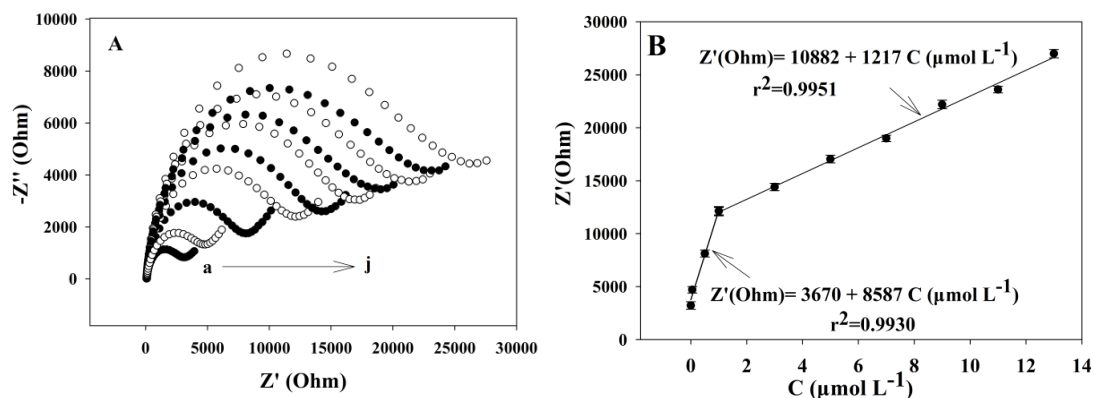


Figure 4. (A) EISs of MIP / Pt NPs-NH₂-r-GO / GCE in 1.0 mmol L⁻¹ K₃Fe(CN)₆+K₄Fe(CN)₆ containing 0.1 mol L⁻¹ KCl after binding in different FP concentrations of 0 (a) ~ 1.3 × 10⁻⁵ mol L⁻¹ (j). (B) The calibration curve of MIP / Pt NPs-NH₂-r-GO / GCE for FP. Error bars represent SD (n= 3).

3.4 Stability reproducibility and selectivity, of the MIP sensor

To evaluate the performance of the as-prepared MIP sensor, selectivity, reproducibility, and stability were next assessed. For the selectivity experiments, bixafen and pyraclostrobin were selected as the interference agents. It had the expected response when using the MIP sensor to measure 1.0 × 10⁻⁶ mol L⁻¹ FP. However, it had a negligible response when using it to measure a 10-fold concentration of either bixafen or pyraclostrobin. The responses were primarily due to the presence of FP when using it to detect its coexistence (i.e., 1.0 × 10⁻⁶ mol L⁻¹ FP + 1.0 × 10⁻⁵ mol L⁻¹ bixafen and 1.0 × 10⁻⁶ mol L⁻¹ FP + 1.0 × 10⁻⁵ mol L⁻¹ pyraclostrobin). Collectively, these results indicated that MIP plays a critical role in the selectivity of the electrochemical sensor (Figure S4).

The stability and repeatability of the MIP sensor were first explored using 1.0 × 10⁻⁶ mol L⁻¹ of FP, resulting in a variation coefficient of 3.5% (n= 5). The Ret of the MIP sensor was maintained at 94.9% of its original value after 20 successive assays. The sensor was then maintained for 4 weeks at room temperature to explore its stability. Result indicated that the Ret of the MIP sensor was maintained at 94.0% (RSD= 4.1%, n= 5) of its original value. Five different electrodes were independently fabricated to evaluate the reproducibility by following the same procedure. A root square deviation (RSD) of 5.8% was obtained for 1.0 × 10⁻⁶ FP, indicative of reliability of this fabrication method.

3.5 Detection of real samples

To test the practicability of the MIP sensor in real samples, recovery tests for FP in vegetables and fruits were next conducted. The samples were treated according to a previous report [22] and results are shown in Table 2. Recoveries were within the range of 96-112%. LC-MS / MS analysis further confirmed the recovery tests according to previously published work [22], consistent with the

MIP sensor data presented in Table 3, which indicated that the sensor was an excellent, practical option to detect FP in real samples.

Table 2. Recovery tests for FP in real samples by MIP sensor

Samples	Added ($\mu\text{mol L}^{-1}$)	Found ($\mu\text{mol L}^{-1}$)	Recovery (%)	RSD (% , n= 5)
	0.00	0.00		
Apple	0.50	0.48	96	4.1
	2.00	2.08	104	2.9
	0.00	0.34		4.5
Cabbage	0.50	0.90	112	4.9
	1.00	1.40	106	3.8

Table 3. LC-MS / MS method for FP in different samples

Samples	Added ($\mu\text{mol L}^{-1}$)	Found ($\mu\text{mol L}^{-1}$)	Recovery (%)	RSD (% , n= 5)
	0.00	0.00		
Apple	0.50	0.52	104	6.3
	2.00	1.95	97.5	5.7
	0.00	0.38		6.4
Cabbage	0.50	0.95	114	5.6
	1.00	1.48	110	6.2

4. CONCLUSION

In this work, we used an easy method to prepare large amounts of Pt NPs with ultrasmall diameters (2-3 nm), which were then loaded onto NH_2 -r-GO using HDPC as the structure-directing agent along with the interreaction between the amino group and Pt. The resulting product was then used to modify an electrode to provide a large surface area and electrical conductivity for MIP. 6-IAA was also used as a novel, functional monomer to construct an electrochemical sensor for FP. The final MIP had a three-dimensional, porous structure, which endowed the as-prepared sensor with excellent performance in the detection of FP. Collectively, these results indicated the utility of this type of sensor for detecting FP in real samples.

ELECTRONIC SUPPLEMENTARY INFORMATION

1. Optimization of assay conditions

We changed the mole ratio of template molecule to functional monomer from 1:1 to 1:6. The Ret value increased with this ratio decreased and a maximum value was obtained at 1:4; after, the Ret

value decreased (Fig. S3A). The effect of electrochemical polymerization time and MIP sensory response was recorded across a range of 8-20 cycles (Fig. S3B). As the polymerization time ranged from 8 to 16 cycles, the response increased, after which the response decreased. This observation was ascribed to the variety of recognition sites. The increase of polymerization time increased recognition sites, but also caused an increase of film thickness. As a result, recognition sites were buried in the MIP. Thus, 16 cycles was selected as the polymerization time.

To determine the effect of adsorption time for MIP sensor response, time was varied from 60 s to 420 s (Fig. S3C). Results indicated that the response leveled off as adsorption time reached 300 s and at a higher concentration level (e.g. 1.0×10^{-6} mol L⁻¹) of FP. Adsorption time was lengthened to 360 s at a low concentration (e.g. 5.0×10^{-8} mol L⁻¹). Thus, we chose 360 s as the optimal adsorption time, which ensured the MIP sensor had enough time to capture FP at a lower concentration.

2. Supplementary Figures

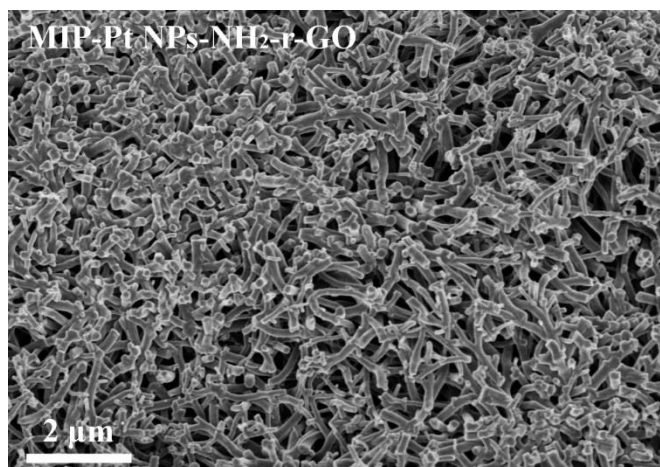


Fig. S1. SEM image of MIP-Pt NPs-NH₂-r-GO /GCE under low magnification.

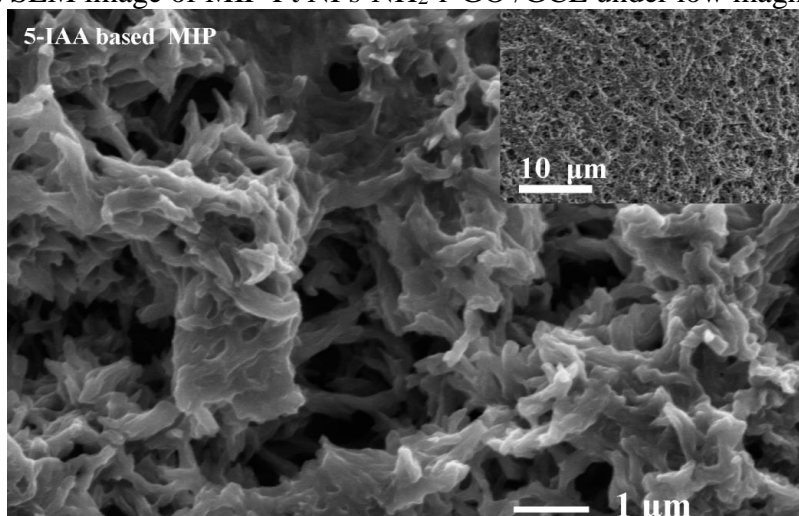


Fig. S2. SEM image of MIP for florfenicol using 5-IAA as the functional monomer.

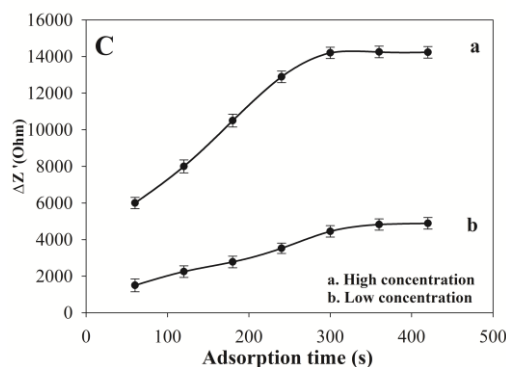


Fig. S3. Effect of different factors on the MIP sensor for 1.0×10^{-6} mol L⁻¹ FP. All error bars represent SD (n= 3). (A) Ratio of template molecule to functional monomer; (B) Electrochemical polymerization time; (C) Adsorption time (a: 1.0×10^{-6} mol L⁻¹; b: 5.0×10^{-8} mol L⁻¹ FP).

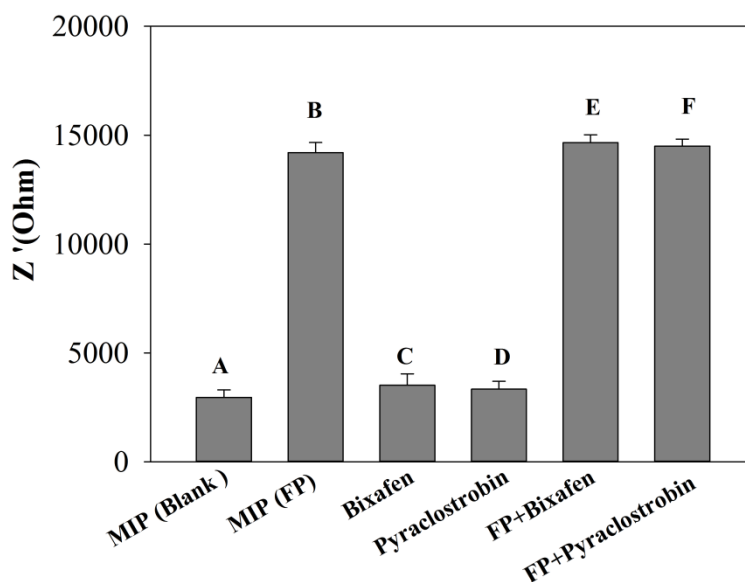


Fig. S4. Influence of similar compounds on FP. Error bars represent SD, n=3. Solution composition: (A) 1.0×10^{-6} mol L⁻¹ FP, (B) 1.0×10^{-5} mol L⁻¹ bixafen, (C) 1.0×10^{-5} mol L⁻¹ pyraclostrobin, (D) A + 1.0×10^{-5} mol L⁻¹ bixafen and (E) A + 1.0×10^{-5} mol L⁻¹ pyraclostrobin.

ACKNOWLEDGEMENTS

This work was jointly supported by Yunnan Province Young Academic and Technical Leaders (2018HB005), the National Natural Science Foundation of China (Grant Nos. 21665008, 21277105), Scientific Research Fundation of Yunnan Education Department (2020J0672), and Scientific Research Fund Project of Honghe University (XJ16B04).

References

1. F. Dong, X. Chen, X. Liu, J. Xu, Y. Li, W. Shan and Y. Zheng, *J. Chromatogr. A.*, 1262 (2012) 98.
2. H. Lin, F. Lin, J. Yuan, F. Cui and J. Chen, *Sci. Total Environ.*, 769 (2021) 144519.
3. A. Crépet, T. M. Luong, J. Baines, P. E. Boon, J. Ennis, M. Kennedy, I. Massarelli, D. Miller, S. Nako, R. Reuss, H. J. Yoon and P. Verger, *Food Control*, 121 (2021) 107563.

4. Y. Shen, Z. Li, Q. Ma, C. Wang, X. Chen, Q. Miao and C. Han, *J. Agric. Food Chem.*, 64 (2016) 3901.
5. A. Abad-Fuentes, E. Ceballos-Alcantarilla, J. V. Mercader, C. Agulló, A. Abad-Somovilla and F. A. Esteve-Turrillas, *Anal. Bioanal. Chem.*, 407 (2015) 4207.
6. F. Tian, C. Qiao, J. Luo, L. Guo, T. Pang, R. Pang, J. Li, C. Wang, R. Wang and H. Xie, *J. Chromatogr. B*, 1152 (2020) 122261.
7. W. Wang, X. Wang, N. Cheng, Y. Luo, Y. Lin, W. Xu and D. Du, *TrAC Anal. Chem.*, 132 (2020) 116041.
8. F. Zhao, J. Wu, Y. Ying, Y. She, J. Wang and J. Ping, *TrAC Anal. Chem.*, 106 (2018) 62.
9. X. Hou, H. Xu, T. Zhen and W. Wu, *Trends Food Sci. Technol.*, 105 (2020) 76.
10. P. Rebelo, E. Costa-Rama, I. Seguro, J. G. Pacheco, H. P. A. Nouws, M. N. D. S. Cordeiro and C. Delerue-Matos, *Biosens. Bioelectron.*, 172 (2021) 112719.
11. M. Mahmoudpour, M. Torbati, M.-M. Mousavi, M. de la Guardia and J. Ezzati Nazhad Dolatabadi, *TrAC Anal. Chem.*, 129 (2020) 115943.
12. F. Zouaoui, S. Bourouina-Bacha, M. Bourouina, N. Jaffrezic-Renault, N. Zine and A. Errachid, *TrAC Anal. Chem.*, 130 (2020) 115982.
13. A. Fan, G. Yang, H. Yang and F. Zhao, *Mater. Today Commun.*, 25 (2020) 101448.
14. L. Yang, B. Zhang, B. Xu, F. Zhao and B. Zeng, *Talanta*, 224 (2021) 121845.
15. L. Guo, H. Zheng, C. Zhang, L. Qu and L. Yu, *Talanta*, 210 (2020) 120621.
16. K. Parate, C. Karunakaran and J. C. Claussen, *Sensor. Actuator. B Chem.*, 287 (2019) 165.
17. Q. Guo, F. Hu, X. Yang, J. Yang, S. Yang, X. Chen, F. Wu and S. D. Minteer, *Microchem. J.*, 158 (2020) 105254.
18. G. Yang and F. Zhao, *J. Mater. Chem. C*, 2 (2014) 10201.
19. Chun Yang, X. F. Ji, W. Q. Cao, J. L. Wang, Q. Zhang, T. L. Zhong and Y. Wang, *Sensor. Actuator. B Chem.*, 282 (2019) 818.
20. F. Zouaoui, S. Bourouina-Bacha, M. Bourouina, I. Abroa-Nemeir, H. Ben Halima, J. Gallardo-Gonzalez, N. E. A. El Hassani, A. Alcacer, J. Bausells, N. Jaffrezic-Renault, N. Zine and A. Errachid, *Sensors Actuators B: Chem.*, 309 (2020) 127753.
21. B. Khadro, C. Sanglar, A. Bonhomme, A. Errachid and N. Jaffrezic-Renault, *Procedia Engineering*, 5 (2010) 371.
22. S. Li, X. Liu, Y. Zhu, F. Dong, J. Xu, M. Li and Y. Zheng, *J. Chromatogr. A.*, 1358 (2014) 46